IEEE Access
Multidisciplinary | Rapid Review | Open Access Journal

Received 25 October 2023, accepted 21 December 2023, date of publication 25 December 2023,
date of current version 19 January 2024.

Digital Object Identifier 10.1109/ACCESS.2023.3346951

RESEARCH ARTICLE

Flying Capacitor Voltage Regulation for a Self-Voltage-Boosting AC Motor Drive

HAOYU WANG[1], MOHAMMED ALKAHTANI[2], (Member, IEEE), JIADONG LU[3], (Senior Member, IEEE), AND YIHUA HU[4], (Senior Member, IEEE)

[1]Shaanxi Huatong Electromechanical Manufacturing Company Ltd., Xi'an 710075, China
[2]Department of Electrical Engineering, College of Engineering, University of Bisha, Bisha 61922, P.O. Box 551, Saudi Arabia
[3]School of Automation, Northwestern Polytechnical University (NWPU), Xi'an 710129, China
[4]Department of Engineering, King's College London, WC2R 2LS London, U.K.

Corresponding author: Mohammed Alkahtani (mskahtani@ub.edu.sa)

This work was supported by the Deanship of Scientific Research at the University of Bisha, Saudi Arabia, through the Promising Program, under Grant UB-Promising-38-14455.

ABSTRACT In order to extend motor operation range, a self-voltage-boosting AC motor drive is proposed in this paper. Compared with the traditional frontend DC-DC converters, the proposed topology reuses the power switches inherently involved within the three-phase inverter without using any additional active components. By modifying the time distribution of the two zero vectors in traditional seven-segment space vector pulse width modulation (SVPWM) technology, the inductor current and the flying capacitor voltage can be adjusted. The proposed topology has the advantage of a wider operating range without extra cost. Moreover, the performance of the motor drive is not affected. Experimental results demonstrate the correctness of the proposed topology.

INDEX TERMS Interior permanent magnet synchronous motor (IPMSM), inverter, voltage bootstrap, flying capacitor.

I. INTRODUCTION

With the fast development of electric drives in industrial and household appliances, the interior permanent magnet synchronous motor (IPMSM) together with whose drive technologies are gaining even more attention than ever [1], [2], [3], [4]. Among all the key technologies, the voltage utilization become one of the most essential factors that affect the motor performance due to the influence of back electromotive force (EMF) of the permanent magnet (PM) machines [5], [6], [7]. Usually, the maximum output speed range of an IPMSM drive much depends on the DC-bus voltage and its utilization factor by taking the flux-weakening control out of consideration. Therefore, it is important to increase the DC-bus voltage utilization factor to extend the motor operation range [8], [9], [10].

Over the years, many solutions have been proposed to increase the voltage utilization of voltage source inverter fed motor drives, achieving higher operating speed range. Adding DC/DC voltage boosting circuit at the front-end of the motor drive is one of the typical techniques to increase the input voltage value of the inverter, thus extending the motor speed [11], [12], [13], [14]. In [11], a new topology of clamped diode multilevel DC/DC converter for a DC motor system is proposed, which reduce current ripples and torque ripples. An improved charge-pump circuit is raised in [12] by using supercapacitors. By controlling the switching states of the power switches in the proposed circuit, the supercapacitors can either be bypassed or be connected in series into the circuit in positive and negative directions, thus generating different DC-link voltages. In [13], an interleaved two leg bidirectional DC/DC converter is utilized in the IPMSM drive, which can boost the DC-link voltage according to the working conditions of the motor but also allowing power been transferred back into the battery. An active power decoupling circuit is proposed in [14] to regulate the DC-link voltage without using electrolytic capacitors. The circuit consists of two parts: one is actually the boost converter and the other is the buck-boost converter. The converters are connected in series for even higher DC-link voltage. Also, the second

The associate editor coordinating the review of this manuscript and approving it for publication was Zhilei Yao.

converter can generate complementary voltage to eliminate voltage ripples of the boost converter. Despite the advantages of increasing the DC-link voltage, thus expanding the operating range of PM motors, these solutions require additional power switches, which might limit their applications.

Open-end winding motor is another solution to extend the operating speed range by introducing an additional inverter [15], [16], [17], [18], [19], [20], [21], [22]. In [15], the zero-sequence current is eliminated in a dual-inverter open-end winding motor drive with common DC-bus using an improved pulse-width modulation (PWM) strategy. The voltage boosting and regulation methods are investigated in [16] by adjusting the fundamental phase angle difference between the two inverters and modify the PWM scheme, respectively. To further extend the open-end winding motor speed range, in [17], the flux weakening control by the fully utilization of the main converter is investigated, where the additional voltage boost is also obtained. The fault-tolerant control of the open-end winding motor drive is researched in [18] against the open-circuit fault of the inverter. To improve the efficiency of the system in open-end winding motor drives, the DC-link voltage is regulated in [19], leading to an increased efficiency of 60% at most. In [20], improved control strategy is proposed to reduce the switching action times of the dual-inverter system. Although the open-end winding motor and the dual-inverter system gain great advantages of higher voltage utilization factor and control adaptability, an additional inverter is required compared with the traditional three-phase IPMSM drive, which might limit their applications [21].

Other topologies like the multilevel converters are popular and suitable for the high voltage/power motor drive applications due to the great benefit of the multiple output voltage levels and the reduced voltage stress on the power switches [23]. However, the multilevel converters usually require more power switches than the conventional three-phase inverter, which will inevitably add additional cost to the system [24], [25], [26]. The flying capacitor assisted two arm inverter motor drive is proposed in [27], which boosts the voltage using the capacitor acrossing two phases of the motor windings. Besides, the voltage stress on the power switches is not increased. However, the application of this strategy might be limited due to the uncommon topology.

To extend the operating speed range of IPMSM drives, many solutions have been proposed either to boost the DC-link voltage using the front-end DC/DC converter or to use specific drive topologies, leading to an increased use of the additional power switches or higher power sources as shown in Fig. 1, where U and E stands for the input voltage and back electromotive force (EMF) of the motor, K_e is the EMF constant, n represents the motor speed. Therefore, in order to tackel the challenge of low cost, modular structure and high efficiency to boost bus voltage, in this paper, a flying capacitor voltage regulation strategy for a self-voltage-boosting IPMSM drive is proposed, where the capacitor is connected in series with the power supply. Compared with the conventional three-phase IPMSM drive,

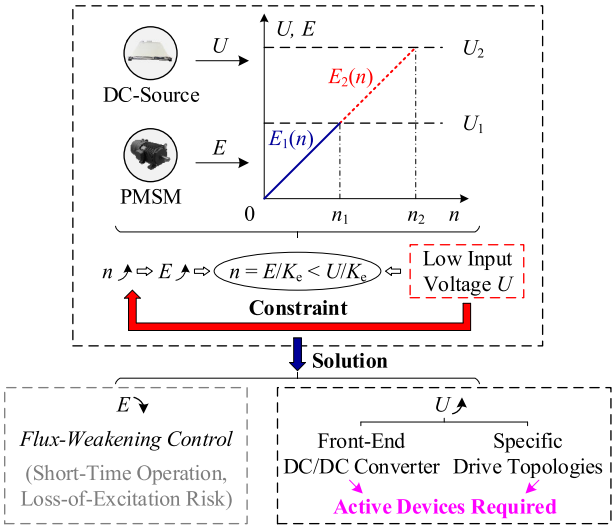

FIGURE 1. Motor operating speed range extending methods.

the proposed topology does not require additional power switches apart from the auxiliary inductors. Benefit from the dynamic adjustment of the time distribution of the two zero voltage vectors, the voltage boosting ratio can be controlled. In addition, since the proposed strategy does not adjust the active voltage vectors, the normal operations of the motor is not affected.

The remainder of this paper is organized as follows. The proposed topology and equivalent circuits are illustrated in Section II. The dynamic adjustment of action time distribution of the zero vectors is elaborated in Section III. The calculation method of the auxiliary inductors current ripples is presented in Section IV. The overall control strategy and discussions are presented in Section V. Experimental validation is presented in Section VI. The conclusion is given finally in Section VII.

II. PROPOSED TOPOLOGY AND WORKING PRINCIPLE

A. PROPOSED TOPOLOGY

The proposed voltage boost topology for a three-phase IPMSM drive is given in Fig. 2. In Fig. 2, C_1 is the flying capacitor, which is used to boost the input voltage value of the inverter. Whereas C_2 stands for the support capacitor of the DC power supply of U_{DC}. u_{C1} and u_{C2} are the voltages of C_1 and C_2, respectively. $S_1, \ldots, S_6$ are the six power switches of the inverter. L_{A1}, L_{B1} and L_{C1} denote the auxiliary inductors, respectively, where i_{LA1}, i_{LB1} and i_{LC1} are the corresponding currents and i_L is the sum of the three currents. i_A, i_B and i_C are the three-phase currents of the IPMSM. The positive directions of the current are along with the arrows shown in Fig. 2.

In the proposed topology, the three auxiliary inductors are used to generate a continuous charging current i_L for the voltage regulation of the flying capacitor C_1. Thus, the power of the DC supply U_{DC} can be transferred to C_1, resulting in the input voltage value of the inverter been boosted from U_{DC} to $(u_{C1} + u_{C2})$. Therefore, the operating speed range of the

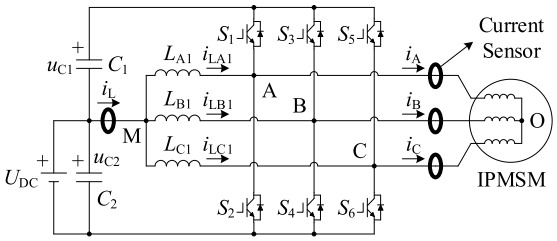

FIGURE 2. Proposed voltage boost topology for IPMSM drives.

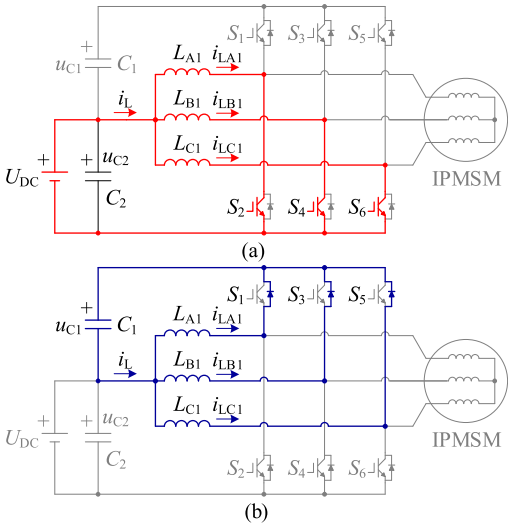

FIGURE 3. Proposed voltage boost topology for IPMSM drives.

motor can be extended. It should be noted that in the proposed topology the flying capacitor C_1 actually provides the voltage level and the reactive power, all the active power comes from the only power source U_{DC}.

B. WORKING PRINCIPLE AND EQUIVALENT CIRCUITS

In traditional three-phase IPMSM drives the inverter consists of six power switches, which is used to control the motor with space vector pulse width modulation (SVPWM) technology. In Fig. 2, the three auxiliary inductors are also connected to the output terminals of the inverter in the proposed topology, therefore, the switching actions of the power switches will lead to the charging or discharging states of the inductors as presented in Fig. 3.

In Fig. 3, the switching states of V_{000} and V_{111} are taken as an example for the analysis of the charging principle. When the lower power switches of the three bridge arms are turned on, the equivalent circuit is shown in Fig. 3(a), where the inductors are charged by the DC power supply and the inductor currents are increased accordingly. Whereas in Fig. 3(b), when all the power switches are turned off or under switching states of V_{111}, the capacitor C_1 will be charged by the auxiliary inductors. Therefore, by properly controlling the switching states of the inverter, the voltage of the flying capacitor can be adjusted which is actually the buck-boost converter. However, as the main purpose of the inverter is to control the motor by generating suitable voltage vectors and

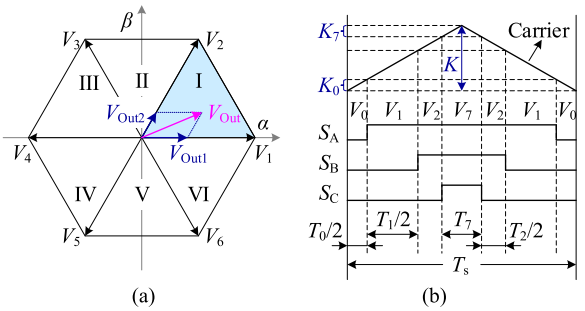

FIGURE 4. Output voltage sectors and seven-segment SVPWM waveform: (a) division of voltage sectors, (b) PWM waveform in sector I.

TABLE 1. Action basic voltage vectors in different sectors.

Sector	Zero Vectors	Active Vectors	Equivalent Duty Cycle		
			Phase-A	Phase-B	Phase-C
I	V_0 & V_7 ($T_0 = T_7$)	V_1 & V_2	T_0/T_s	$(T_0+T_1)/T_s$	$1\text{-}T_7/T_s$
II		V_2 & V_3	$(T_0+T_3)/T_s$	T_0/T_s	$1\text{-}T_7/T_s$
III		V_3 & V_4	$1\text{-}T_7/T_s$	T_0/T_s	$(T_0+T_3)/T_s$
IV		V_4 & V_5	$1\text{-}T_7/T_s$	$(T_0+T_5)/T_s$	T_0/T_s
V		V_5 & V_6	$(T_0+T_5)/T_s$	$1\text{-}T_7/T_s$	T_0/T_s
VI		V_6 & V_1	T_0/T_s	$1\text{-}T_7/T_s$	$(T_0+T_1)/T_s$

the basic voltage vectors not only contain the aforementioned two zero vectors, the regulation strategy of the capacitor voltage is different from the traditional buck-boost converter, which will be further analyzed in the remaining parts of the paper.

III. PROPOSED DYNAMIC ADJUSTMENT OF ACTION TIME DISTRIBUTION OF TWO ZERO VOLTAGE VECTORS

A. VOLTAGES ON AUXILIARY INDUCTORS

As mentioned above, according to different switching states, the basic voltage vectors of the three-phase inverter contain not only the two zero vectors V_{000} (V_0), V_{111} (V_7), but also other six active voltage vectors, namely, V_{100} (V_1), V_{110} (V_2), V_{010} (V_3), V_{011} (V_4), V_{001} (V_5), and V_{101} (V_6). The output voltage range is divided into six sectors (I, II, …, VI) by the boundaries of these six active vectors and the output voltage vector is generated by several basic voltage vectors in each pulse width modulation (PWM) cycle. The division of the sectors and the traditional seven-segment SVPWM technology are illustrated in Fig. 4, where S_A, S_B, and S_C are the switching states of the three bridge arms, T_0, …, T_7 represent the action time of the eight basic voltage vectors, T_s is the PWM cycle period. It can be seen from Fig. 4 that the switching states of the inverter in each sector contain different active basic voltage vectors, which are given in Table 1.

By adding active voltage vectors into the PWM cycle, the control strategy of regulating u_{C1} is completely different from that of the traditional buck-boost converter. It can be seen from Table 1 that the equivalent duty cycle of the buck-boost conversion for the three phases in each sector are different. However, the trajectory of the output voltage vector is a circular one, therefore, the sector will pass through I, II, …,

to VI in sequence, and then back to sector I again. For each phase of the bridge arm, the voltage on the auxiliary inductor caused by active voltage vectors is actually a sinusoidal one. This can also be explained by the line voltages of the motor, i.e., u_{AB}, u_{BC} and u_{CA}, which are sinusoidal ones as shown in Fig. 2. Because the line voltages of the auxiliary inductors are the same with that of the motor, the AC component of the phase voltages of the three inductors u_{AM_AC}, u_{BM_AC} and u_{CM_AC} caused by active voltage vectors are also sinusoidal ones as illustrated in (1)

$$\begin{cases} u_{AM\_AC} = U \cdot \sin(2\pi f \cdot t) \\ u_{BM\_AC} = U \cdot \sin(2\pi f \cdot t - 2\pi/3) \\ u_{CM\_AC} = U \cdot \sin(2\pi f \cdot t + 2\pi/3) \end{cases} \tag{1}$$

where U stands for the amplitude of the phase voltage on the motor windings and the inductors, f is the fundamental frequency of the phase voltage of the motor, t stands for time.

It should be noted that in (1), the voltages of the inductors are the fundamental voltage, which stands for the equivalent voltage generated by the active voltage vectors. Also, as the impact of DC voltage component of the three inductors can be compensated by the zero vectors, which is not considered in (1). Thus, the average voltages caused by the active vectors of the inductors during one fundamental period T_f ($T_f = 1/f$) can be calculated using (2).

$$\begin{cases} u_{AM\_AC\_AVG} = \int_0^{T_f} u_{AM\_AC} dt = 0 \\ u_{BM\_AC\_AVG} = \int_0^{T_f} u_{BM\_AC} dt = 0 \\ u_{CM\_AC\_AVG} = \int_0^{T_f} u_{CM\_AC} dt = 0 \end{cases} \tag{2}$$

where $u_{AM\_AC\_AVG}$, $u_{BM\_AC\_AVG}$ and $u_{CM\_AC\_AVG}$ are the average voltages caused by the active voltage vectors of the inductors during one fundamental period.

On the other hand, the voltages u_{AM_ZERO}, u_{BM_ZERO} and u_{CM_ZERO} of the inductors caused by the two zero vectors can be calculated using (3)

$$\begin{aligned} u_{AM\_ZERO} &= u_{BM\_ZERO} = u_{CM\_ZERO} \\ &= (u_{C1} \cdot T_7 - u_{C2} \cdot T_0)/T_s \end{aligned} \tag{3}$$

From the above analysis it can be seen that the average voltages of the inductors during one fundamental period are the same as given in (3). Therefore, it is possible to control the voltages on the auxiliary inductors by modifying the time distribution of T_0 and T_7.

B. PROPOSED DYNAMIC ADJUSTMENT OF TIME DISTRIBUTION OF TWO ZERO VOLTAGE VECTORS

The charging current i_L can be regulated by modifying the voltages of the inductors. The total action time of the zero voltage vectors determines the value of the output voltage, whereas the time distribution of T_0 and T_7 does not affect the value of the output voltage. As a result, according to (3):

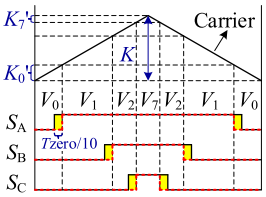

FIGURE 5. SVPWM waveform using the proposed dynamic adjustment strategy in sector I.

1) The charging current i_L can be increased by extending the action period of T_0, whereas shortening T_7.

2) The charging current i_L can be decreased by shortening the action period of T_0, whereas extending T_7.

For example, if T_0 takes 70% of the action time of zero vectors and T_7 takes 30%, the SVPWM waveform using the proposed dynamic adjustment strategy is shown in Fig. 5. The yellow shading areas denotes the dynamic adjustment of time distribution of two zero voltage vectors, and the width can be calculated by [T_{ZERO}·(70%-30%)/4]. Compared with Fig. 4(b) where $K_0 = K_7$ and $(K_0+K_7)/K = T_{Zero}/T_s$ (T_{Zero} is the action time of zero vectors), in Fig. 5, the relations among the parameters are given in (4). It should be noted that the action time of the active vectors in Fig. 5 are the same as that in Fig. 4(b).

$$\begin{cases} K_0'/70\% = K_7'/30\% = T_{Zero} \\ (K_0' + K_7')/K = (K_0 + K_7)/K = T_{Zero}/T_s \end{cases} \tag{4}$$

It can be seen from Fig. 5 that compared with the traditional SVPWM waveform, the proposed strategy modifies the time distribution of the zero vectors. As a result, the voltages of the inductors can be dynamically adjusted, whereas the actual output voltage of the inverter for motor control remains unchanged and the motor performance will not be affected.

IV. AUXILIARY INDUCTOR CURRENT RIPPLE CALCULATION

From the above analysis, it can be seen that the average voltages of the auxiliary inductors can be adjusted by modification on the time distribution of the zero vectors during each fundamental period T_f, thus the average charging current of i_L can be controlled. However, the transient voltages of the inductors change from time to time, therefore, it is essential to analyze the current ripples of the inductors. It should be noted that the impact of the zero vectors on the current ripples are similar to that of the traditional buck-boost converter, therefore, in this part the impact of the active voltage vectors on the inductor current ripples will be analyzed.

In (1), the instantaneous voltages of the inductors caused by the active vectors are sinusoidal ones, therefore, the

corresponding current ripples can be calculated using (5).

$$\begin{cases} \Delta i_{\mathrm{LA1}} = \int_0^{\frac{T_f}{2}} \frac{u_{\mathrm{AM\_AC}}}{L_{\mathrm{A1}}} dt = \frac{U \cdot T_f}{\pi L_{\mathrm{A1}}} = \frac{U_{\mathrm{L}} \cdot T_f}{\sqrt{3}\pi L_{\mathrm{A1}}} \\ \Delta i_{\mathrm{LB1}} = \frac{U \cdot T_f}{\pi L_{\mathrm{B1}}} = \frac{U_{\mathrm{L}} \cdot T_f}{\sqrt{3}\pi L_{\mathrm{B1}}} \\ \Delta i_{\mathrm{LC1}} = \frac{U \cdot T_f}{\pi L_{\mathrm{C1}}} = \frac{U_{\mathrm{L}} \cdot T_f}{\sqrt{3}\pi L_{\mathrm{C1}}} \end{cases} \tag{5}$$

where Δi_{LA1}, Δi_{LB1} and Δi_{LC1} are the current ripples (peak-peak value) of the three inductances L_{A1}, L_{B1} and L_{C1}, U_{L} represents the amplitude of the line voltages of motor drive.

Therefore, the current ripples caused by the active voltage vectors is given by (6)

$$\begin{cases} i_{\mathrm{LA1\_AC}} = -\frac{U_{\mathrm{L}} \cdot T_f}{2\sqrt{3}\pi L_{\mathrm{A1}}} \cdot \cos\left(2\pi f \cdot t\right) \\ i_{\mathrm{LB1\_AC}} = -\frac{U_{\mathrm{L}} \cdot T_f}{2\sqrt{3}\pi L_{\mathrm{B1}}} \cdot \cos\left(2\pi f \cdot t - 2\pi/3\right) \\ i_{\mathrm{LC1\_AC}} = -\frac{U_{\mathrm{L}} \cdot T_f}{2\sqrt{3}\pi L_{\mathrm{C1}}} \cdot \cos\left(2\pi f \cdot t + 2\pi/3\right) \end{cases} \tag{6}$$

where $i_{\mathrm{LA1\_AC}}$, $i_{\mathrm{LB1\_AC}}$ and $i_{\mathrm{LC1\_AC}}$ are the AC component of the instantaneous inductor currents.

It can be seen from (5) and (6) that the amplitude of current ripples is proportional to the value of $U_{\mathrm{L}} \cdot T_f$, which is mainly determined by the motor parameters as shown in (7)

$$U_{\mathrm{L}} \cdot T_f = U_{\mathrm{L}}/f = 60U_{\mathrm{L}}/np \tag{7}$$

where n and p are the motor speed and pole pairs.

Usually, the amplitude of line voltage U_{L} has similar values with the amplitude of line EMF E_{L} in IPMSM drives, therefore, the value of $U_{\mathrm{L}} \cdot T_f$ can be calculated as shown in (8)

$$U_{\mathrm{L}} \cdot T_f \approx E_{\mathrm{L}}/f = \left(\sqrt{3} \cdot \sqrt{2}\pi N k f \Phi_1\right)/f \approx 7.7 N k \Phi_1 = \lambda \tag{8}$$

where N and k are the turns-in-series per-phase and winding factor of the motor, respectively, which are all constant values. Φ_1 represents the per pole flux, which is usually constant value for PM machines, λ is a constant value.

It can be seen that the value of $U_{\mathrm{L}} \cdot T_f$ in (8) is approximately equal to a constant value λ, which is mainly determined by the motor parameters.

V. OVERALL CONTROL STRATEGY AND DISCUSSIONS

A. OVERALL CONTROL STRATEGY

The overall control strategy is illustrated in Fig. 6, where n^* and n are the motor speed command and actual value, θ is the rotor position, i_{ABC} is the three-phase currents of the motor, K_{A}, K_{B}, K_{C} and K_{A}', K_{B}', K_{C}' are the original and modified three comparator values for the generating of PWM signals, $u_{\mathrm{C1}}{}^*$ denotes the command value of u_{C1}.

In Fig. 6, the only difference from the proposed controller and the traditional one is the modification of the three comparator values for the generating of PWM signals. It can be noted that the increase in the comparison value of the three-phase PWM signal is the same. Therefore, this

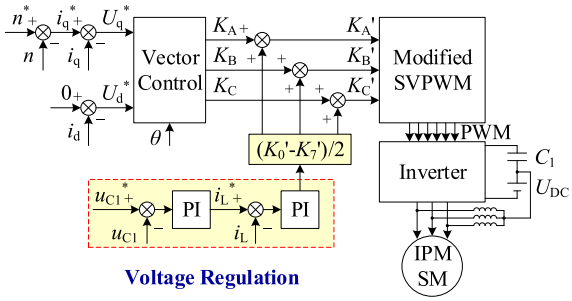

FIGURE 6. Overall control strategy.

modification only change the time allotment of T_0 and T_7, whereas the action time of the total zero voltage vector and active vectors remain unchanged. From the perspective of motor control itself, the control performance is not affected. Thus, the speed and current controller parameters show no significant differences with that of the traditional controller.

In terms of voltage modulation, as the time allotment of T_0 and T_7 directly affect the action time of the upper and lower power switches. The proposed controller utilize a voltage-current double closed-loop controller. The control target is to ensure that the voltage of the upper capacitor is equal to the voltage of the lower capacitor, which adopts a PI controller. Subsequently, in order to achieve that goal, the current of the three-phase inductors are adjusted by another PI controller. The adjustment value of the three comparators are finally obtained.

Compared with the traditional controller, the proposed one adds a voltage regulation modular (presented in FIGURE 6 in the manuscript). Therefore, the computational burden of the proposed method is slightly increased due to the use of two PI controllers. This is the drawback of the proposed controller. However, as the fast development of micro-controllers, the slightly increased computational burden has limited impact on modern digital signal processors (DSPs), e.g., TMS320F28335 in experimental setup. Also, considering the advantages of a wider operation range, the proposed controller remains attractive.

B. DISCUSSIONS

As the increase of the input voltage of the inverter, the motor operating speed range will be extended. However, because the inductor current is adjusted by modifying the time distribution of the zero vectors as given in (3) and Fig. 5, the action time of the active voltage vectors will be shortened. Therefore, it is essential to analyze the maximum action time of the active voltage vectors.

In fact, from the above analysis it can be seen that the equivalent duty cycle is determined by the action time of both the active and the zero voltage vectors. During one fundamental period, the influence of the active voltage vectors on the inductors is same as that when $T_0 = T_7$. Therefore, for the buck-boost conversion, the equivalent duty cycle α can

be calculated as in (9)

$$\alpha = \frac{T_{\text{Lower}}}{T_s} = \frac{T_0 + [T_s - (T_0 + T_7)]/2}{T_s} = \frac{1}{2} + \frac{T_0 - T_7}{2T_s} \tag{9}$$

where T_{Lower} stands for the action time of the equivalent lower power switches.

From (9) it can be seen that: 1) At the first beginning of the capacitor charge period, the action time of T_7 should be equal to T_s and α is 0. 2) As the action time of T_0 increases, the voltage of u_{C1} gradually rises. 3) When T_0 is equal to T_7, α is 0.5 and the voltage of both capacitors will be the same.

The input voltage of the inverter is the sum of u_{C1} and u_{C2}, which is given in (10).

$$\begin{aligned} u_{C1} + u_{C2} &= \frac{\alpha}{1-\alpha} \cdot u_{C2} + u_{C2} = \frac{1}{1-\alpha} \cdot u_{C2} \\ &= \frac{2T_s \cdot u_{C2}}{T_s - (T_0 - T_7)}. \end{aligned} \tag{10}$$

After the precharge of the capacitors, the input voltage of the inverter will be twice as the DC voltage source ($T_0 = T_7$). Theoretically, the action time of the two zero vectors will be the same and therefore the operating speed range of the motor will be doubled. By changing the time distribution of the zero vectors, the voltage of the upper capacitor u_{C1} can be higher than the lower one u_{C2}. Whereas this requires the action time of the two zero vectors being different, meaning that the total action time of the zero vectors cannot be shorter than this time difference as given in (11).

$$T_{\text{ZERO\_MIN}} = |T_0 - T_7| \tag{11}$$

where $T_{\text{ZERO\_MIN}}$ represents the minimum action time of the zero vectors.

The maximum action time of the active vectors is thereby given by (12).

$$T_{\text{ACTIVE\_MAX}} = T_s - T_{\text{ZERO\_MIN}} = T_s - |T_0 - T_7| \tag{12}$$

where $T_{\text{ACTIVE\_MAX}}$ represents the maximum action time of the active vectors.

In order to boost the input voltage of the inverter, the duty cycle α should be bigger than 0.5 in theory. Therefore, $T_{\text{ACTIVE\_MAX}}$ will be T_s-(T_0-T_7), and the maximum active voltage on the motor $u_{\text{ACTIVE\_MAX1}}$ in this condition is given in (13).

$$u_{\text{ACTIVE\_MAX1}} = (u_{C1} + u_{C2}) \cdot T_{\text{ACTIVE\_MAX1}} = 2T_s \cdot u_{C2} \tag{13}$$

where $T_{\text{ACTIVE\_MAX1}}$ stands for the maximum action time of the active vectors during voltage boost condition.

It can be seen from (13) that during voltage boost condition, the maximum active voltage on the motor is a constant value, which will not be affected by the voltage boost factor.

However, when the converter is operating in the buck mode ($T_0 < T_7$), $T_{\text{ACTIVE\_MAX}}$ is $T_s + (T_0$-$T_7)$, and the maximum active voltage on the motor $u_{\text{ACTIVE\_MAX2}}$ in this condition will be (14).

$$\begin{aligned} u_{\text{ACTIVE\_MAX2}} &= (u_{C1} + u_{C2}) \cdot T_{\text{ACTIVE\_MAX2}} \\ &= 2T_s \cdot u_{C2} \cdot \frac{\alpha}{1-\alpha} < 2T_s \cdot u_{C2} \end{aligned} \tag{14}$$

where $T_{\text{ACTIVE\_MAX2}}$ stands for the maximum action time of the active vectors during buck conversion mode.

It can be seen from (14) that during buck conversion, the maximum active voltage is smaller than that during the boost condition in (13), and will be affected by the duty cycle α.

Compared with the traditional DC-DC converters, the voltage boost function proposed in this paper does not rely on any additional active components. This is because the three-phase motor drive is functional reused, which brings the advantage of a wider operating range without extra cost. Also, the motor operating range is significantly extended without the help of additional active components compared with the traditional motor drive.

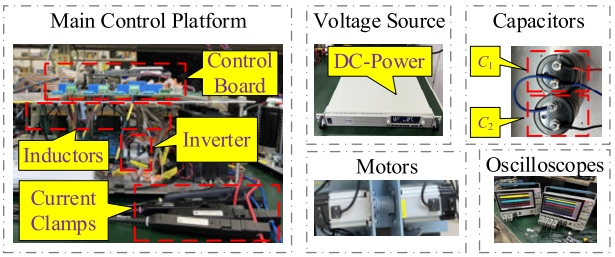

FIGURE 7. Experimental setup.

TABLE 2. Main parameters of the motor.

Parameters	Value
Flux Linkage	1.15 V·s
Rated Current	4 A
Line Resistance	1.16 Ω
d-axis Inductance	1.60 mH
q-axis Inductance	4.11 mH

VI. EXPERIMENTAL VALIDATION

In order to verify the correctness of the proposed topology and control strategy, the experimental setup is shown in Fig. 7. The DC-Power is a TDK G300-11.5-1P208-M voltage source, which is connected to C_2. The capacitance of the flying capacitor C_1 is 3300 μF. The core of the main control board is a digital signal processor, TMS320F28335. The inverter of the motor drive 1 is an Infineon IGBT module (FS100R12KT4) with switching frequency of 10 kHz. The inductance value of the inductors is 50 mH. The current clamps are Tektronix TCP0030A high precision current probes. Two oscilloscopes (Tektronix MOS46 and MSO44) are used for signal sampling and recording. The system variables are also sampled by the oscilloscopes through the digital to analog converters (DACs) of the controller. The load is produced by a generator with the same parameter. Main parameters of the motor are given in Table 2.

The experimental results of the voltage boost function during precharge process are illustrated in Fig. 8, where the

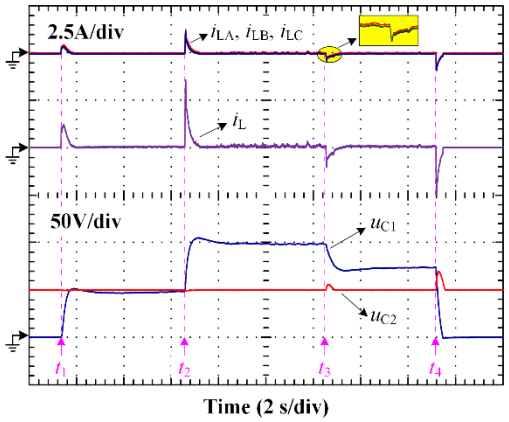

FIGURE 8. Experimental results of the voltage boost function.

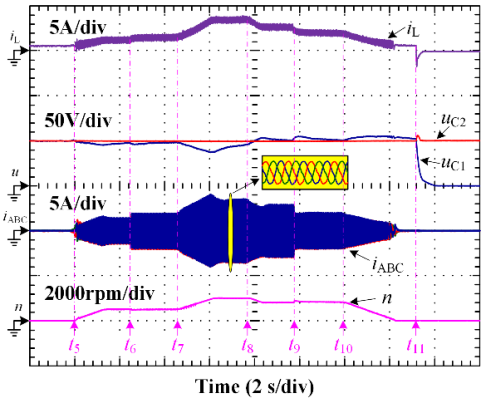

FIGURE 9. Experimental results during normal operations of the motor.

inductor currents and the capacitor voltages are presented. At the beginning, the lower capacitor is charged to 50V as the same voltage value with the DC-source. At t_1, the voltage command of u_{C1} is set the same with the lower capacitor voltage, u_{C1} increases as the inductor current rises. At t_2 and t_3 the command of u_{C1} is set to twice and 1.5 times of u_{C2}, respectively. And finally the voltage command of u_{C1} is set to zero at t_4. This demonstrate the voltage boost function during precharge process of the capacitor. It can be seen from Fig. 8 that the voltage of the upper capacitor follows the command value accurately. Also, this dynamic adjustment only changes the time distribution of the two zero voltage vectors, which does not affect the output active vector.

In order to test the system performances during normal operations of the motor, experimental results are presented in Fig. 9. At the beginning, both the two capacitor voltage are charged to 50V. At t_5, the motor speed command is set to 500 rpm with light load, whereas a heavy load is added at t_6. The speed command is changed to 1000 rpm at t_7 and the load increases as the speed rises. At t_8 the speed changed to 800 rpm and a half load is unloaded at t_9. Finally the speed set to 0 rpm at t_{10} and then the voltage command of u_{C1} is set to 0 V at t_{11}. It can be seen that with the dynamic operation of the motor, the voltage of u_{C1} fluctuates. However, with the help of the auxiliary inductors, the voltage can be controlled within a tolerable value. It should be noted that this ripple is also rated to the PI parameters of the voltage regulation module in Fig. 6.

The experimental results with the closed-loop control of the upper capacitor voltage is presented in Fig. 10, where the motor starts from 0 rpm to 800 rpm and then stops. It can be seen that the voltage of the upper capacitor decreases gradually with the starting of the motor, and then the total inductor current rises due to the closed-loop control of the capacitor voltage. The voltage of the upper capacitor increases subsequently. During stopping of the motor, the upper capacitor voltage increases because of the energy feedback. However, with the help of the closed-loop control strategy, the upper capacitor voltage is controlled to follow the voltage of the lower one.

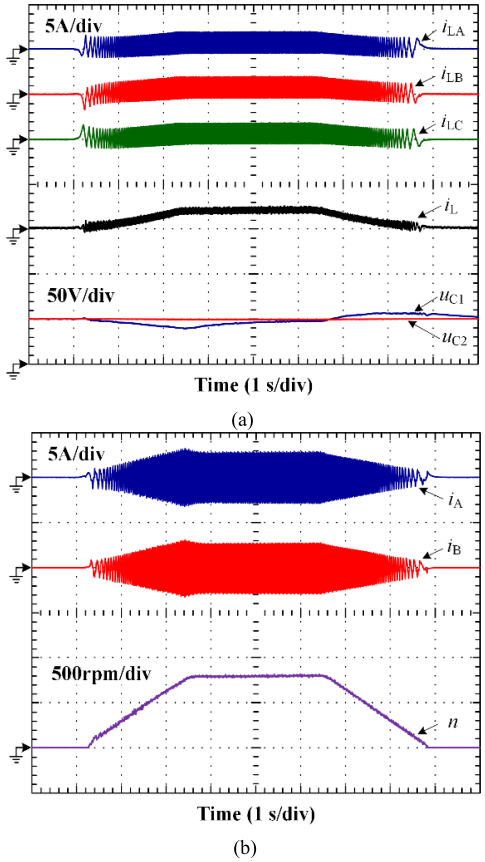

FIGURE 10. Experimental results with closed-loop control of the voltage: (a) inductor currents and capacitor voltages, (b) motor currents and speed.

It can also be seen in Fig. 10(a), the auxiliary inductor currents contain ripples with the fundamental frequency of the motor. This conclusion coincides with the theoretical analysis in Section IV. However, as the total charging current is the sum of the three inductor currents, the current ripple frequency of i_L is 3 times of the fundamental one. Also, the amplitude of the current ripple of i_L is much smaller than the single inductor current due to the symmetrical auxiliary inductor currents i_{LA1_AC}, i_{LB1_AC} and i_{LC1_AC}.

The experimental results of the system performances with the open-loop control of the capacitor voltages is presented

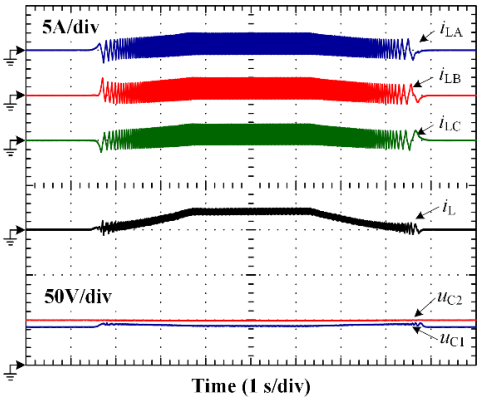

FIGURE 11. Experimental results of the inductor currents and capacitor voltages with open-loop control of the voltage.

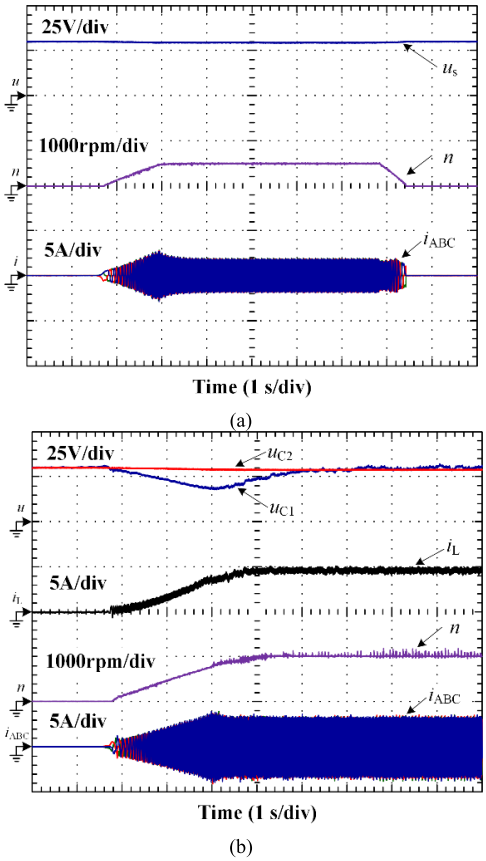

FIGURE 12. Experimental results of the motor performance using: (a) the traditional inverter topology, (b) the proposed topology.

in Fig. 11 (duty cycle is set with the constant value of 0.5), where the motor also starts from 0 rpm to 800 rpm and then stops. It can be seen that without the help of PI closed-loop controller, the voltage of the upper capacitor cannot follow the lower one. This is similar to that of the open-loop control of the DC/DC converters. The motor currents and speed are similar to that with the closed-loop controller.

The comparisons of motor performances between the traditional and proposed topology are illustrated in Fig. 12, where the voltage of the DC source is set 30 V. From the results, it can be seen that the input voltage of the proposed controller reaches approximately 60 V, which is 2 times that of the traditional controller. Therefore, the voltage boost capacity of the proposed controller is demonstrated. The motor speed command is set to a very high value that the motor cannot reach to test the maximum operating speed range. It can be seen from the results that the maximum speed of the motor in traditional topology is about 500 rpm, whereas the speed reaches almost 1000 rpm in the proposed strategy. The motor speed of the proposed controller is nearly 2 times that of the traditional controller, which prove the expansion of the motor operation range.

VII. CONCLUSION

To boost the input voltage of the inverter for IPMSM drives, a flying capacitor voltage regulation strategy is proposed in this paper. The voltage of the flying capacitor is adjusted by controlling the auxiliary inductors that link the inverter and the DC source. The contributions of this paper are listed below:

1) No additional power switches are needed for the voltage boost of the proposed strategy, instead the power switches within the initial inverter is taken full use of.

2) The inductor current is modulated using the proposed time distribution strategy of the two zero vectors, thus the active output vector is not modified and the performance of the motor is not affected.

3) The voltage of the flying capacitor can be controlled the same as the source voltage level, thus the input voltage of the inverter reaches 2 times the source voltage. Therefore, the operation range of the motor can be extended by nearly 2 times compared with the traditional one.

4) Although the voltage gain is usually set twice in the proposed topology, considering the low cost and benefit, the proposed topology still has great appeal.

ACKNOWLEDGMENT

We would like to acknowledge the Deanship of Scientific Research, University of Bisha, for funding this research through the promising program under grant number (UB-Promising-38-1445).

REFERENCES

[1] G. Wang, F. Chen, N. Zhao, Y. Bai, B. Li, S. Liu, and D. Xu, "Current reconstruction considering time-sharing sampling errors for single DC-link shunt motor drives," *IEEE Trans. Power Electron.*, vol. 36, no. 5, pp. 5760–5770, May 2021.

[2] Q. Tang, A. Shen, P. Luo, H. Shen, W. Li, and X. He, "IPMSMs sensorless MTPA control based on virtual q-axis inductance by using virtual high-frequency signal injection," *IEEE Trans. Ind. Electron.*, vol. 67, no. 1, pp. 136–146, Jan. 2020.

[3] W. Chen, S. Zeng, G. Zhang, T. Shi, and C. Xia, "A modified double vectors model predictive torque control of permanent magnet synchronous motor," *IEEE Trans. Power Electron.*, vol. 34, no. 11, pp. 11419–11428, Nov. 2019.

[4] C. Gong, Y. Hu, J. Gao, Y. Wang, and L. Yan, "An improved delay-suppressed sliding-mode observer for sensorless vector-controlled PMSM," *IEEE Trans. Ind. Electron.*, vol. 67, no. 7, pp. 5913–5923, Jul. 2020.

[5] M. O. Badawy, T. Husain, Y. Sozer, and J. A. De Abreu-Garcia, "Integrated control of an IPM motor drive and a novel hybrid energy storage system for electric vehicles," *IEEE Trans. Ind. Appl.*, vol. 53, no. 6, pp. 5810–5819, Nov. 2017.

[6] Y. Lee and J.-I. Ha, "Hybrid modulation of dual inverter for open-end permanent magnet synchronous motor," *IEEE Trans. Power Electron.*, vol. 30, no. 6, pp. 3286–3299, Jun. 2015.
[7] P. R. Kumar, R. S. Kaarthik, K. Gopakumar, J. I. Leon, and L. G. Franquelo, "Seventeen-level inverter formed by cascading flying capacitor and floating capacitor H-bridges," *IEEE Trans. Power Electron.*, vol. 30, no. 7, pp. 3471–3478, Jul. 2015.
[8] G. Wang, H. Hu, D. Ding, N. Zhao, Y. Zou, and D. Xu, "Overmodulation strategy for electrolytic capacitorless PMSM drives: Voltage distortion analysis and boundary optimization," *IEEE Trans. Power Electron.*, vol. 35, no. 9, pp. 9574–9585, Sep. 2020.
[9] S. Du, B. Wu, and N. Zargari, "Delta-channel modular multilevel converter for a variable-speed motor drive application," *IEEE Trans. Ind. Electron.*, vol. 65, no. 8, pp. 6131–6139, Aug. 2018.
[10] G. Han and H. Chen, "Improved power converter of SRM drive for electric vehicle with self-balanced capacitor voltages," *IEEE Trans. Transport. Electrific.*, vol. 7, no. 3, pp. 1339–1348, Sep. 2021.
[11] A. A. A. Ismail and A. Elnady, "Advanced drive system for DC motor using multilevel DC/DC buck converter circuit," *IEEE Access*, vol. 7, pp. 54167–54178, 2019.
[12] H. Matsumoto, Y. Neba, and H. Asahara, "Variable-form carrier-based PWM for boost-voltage motor driver with a charge-pump circuit," *IEEE Trans. Ind. Electron.*, vol. 62, no. 8, pp. 4728–4738, Aug. 2015.
[13] Y.-S. Lin, K.-W. Hu, T.-H. Yeh, and C.-M. Liaw, "An electric-vehicle IPMSM drive with interleaved front-end DC/DC converter," *IEEE Trans. Veh. Technol.*, vol. 65, no. 6, pp. 4493–4504, Jun. 2016.
[14] C. Zhang, L. Xu, X. Zhu, Y. Du, and L. Quan, "Elimination of DC-link voltage ripple in PMSM drives with a DC-split-capacitor converter," *IEEE Trans. Power Electron.*, vol. 36, no. 7, pp. 8141–8154, Jul. 2021.
[15] Z. Shen, D. Jiang, L. Zhu, Y. Xu, T. Zou, Z. Liu, and R. Qu, "A novel zero-sequence current elimination PWM scheme for an open-winding PMSM with common DC bus," *IEEE Trans. Power Electron.*, vol. 34, no. 12, pp. 12476–12490, Dec. 2019.
[16] Z. Huang, T. Yang, P. Giangrande, S. Chowdhury, M. Galea, and P. Wheeler, "An active modulation scheme to boost voltage utilization of the dual converter with a floating bridge," *IEEE Trans. Ind. Electron.*, vol. 66, no. 7, pp. 5623–5633, Jul. 2019.
[17] S. Wdaan, C. Perera, and J. Salmon, "Maximum torque operation of open-winding induction motor dual drives using a floating capacitor bridge in the field weakening region," *IEEE Trans. Power Electron.*, vol. 37, no. 8, pp. 9629–9640, Aug. 2022.
[18] P. Wang, S. Gong, X. Sun, Z. Liu, D. Jiang, and R. Qu, "Fault-tolerant reconfiguration topology and control strategy for symmetric open-winding multiphase machines," *IEEE Trans. Ind. Electron.*, vol. 69, no. 9, pp. 8656–8666, Sep. 2022.
[19] A. Amerise, M. Mengoni, L. Zarri, A. Tani, S. Rubino, and R. Bojoi, "Open-end windings induction motor drive with floating capacitor bridge at variable DC-link voltage," *IEEE Trans. Ind. Appl.*, vol. 55, no. 3, pp. 2741–2749, May 2019.
[20] W. Hu, C. Ruan, H. Nian, and D. Sun, "An improved modulation technique with minimum switching actions within one PWM cycle for open-end winding PMSM system with isolated DC bus," *IEEE Trans. Ind. Electron.*, vol. 67, no. 5, pp. 4259–4264, May 2020.
[21] X. Sun, Z. Liu, D. Jiang, and W. Kong, "Multiphase open-end winding induction machine drive with the floating capacitor," *IEEE Trans. Ind. Appl.*, vol. 56, no. 5, pp. 5013–5022, Sep./Oct. 2020.
[22] Z. Yu, C. Gan, K. Ni, Y. Chen, and R. Qu, "A simplified PWM strategy for open-winding flux modulated doubly-salient reluctance motor drives with switching action minimization," *IEEE Trans. Ind. Electron.*, vol. 70, no. 3, pp. 2241–2253, Mar. 2023, doi: 10.1109/TIE.2022.3165282.
[23] H. Tian and Y. W. Li, "Carrier-based stair edge PWM (SEPWM) for capacitor balancing in multilevel converters with floating capacitors," *IEEE Trans. Ind. Appl.*, vol. 54, no. 4, pp. 3440–3452, Jul./Aug. 2018.
[24] M. Lee, C.-S. Yeh, and J.-S. Lai, "A hybrid binary-cascaded multi-level inverter with simple floating-capacitor-voltage control," *IEEE Trans. Power Electron.*, vol. 36, no. 2, pp. 2218–2230, Feb. 2021.
[25] M. G. Majumder, A. K. Yadav, K. Gopakumar, K. Raj R, U. Loganathan, and L. G. Franquelo, "A 5-Level inverter scheme using single DC link with reduced number of floating capacitors and switches for open-end IM drives," *IEEE Trans. Ind. Electron.*, vol. 67, no. 2, pp. 960–968, Feb. 2020.
[26] S. Du, B. Wu, and N. R. Zargari, "Common-mode voltage elimination for variable-speed motor drive based on flying-capacitor modular multilevel converter," *IEEE Trans. Power Electron.*, vol. 33, no. 7, pp. 5621–5628, Jul. 2018.
[27] K. Lee, "Flying capacitor-assisted two-leg inverter for permanent magnet synchronous motor drive," *IEEE J. Emerg. Sel. Topics Power Electron.*, vol. 9, no. 5, pp. 5429–5440, Oct. 2021.

HAOYU WANG received the B.S. and M.S. degrees in electrical and electronics engineering from the University of Liverpool (UoL), Liverpool, U.K., in 2019 and 2020, respectively. Currently, he is an Electrical Engineer with Shaanxi Huatong Electromechanical Manufacturing Company Ltd. His research interests include motor controller and serve motor control.

MOHAMMED ALKAHTANI (Member, IEEE) received the B.Eng., M.Sc., and Ph.D. degrees in electrical and electronics engineering from Liverpool John Moores University and the University of Liverpool, U.K., in 2014, 2016, and 2021, respectively. He is an Assistant Professor with the Department of Electrical Engineering, College of Engineering, University of Bisha, Bisha, Saudi Arabia. He has more than five years of working experience in the industry worldwide, with many applications of innovative products. His research interests include the management of photovoltaic and PV array efficiency improvement, artificial intelligence, and algorithms for energy management systems. He is an IEEE Young Professional. In 2014, he was a member of the Saudi Council of Engineers (SCE).

JIADONG LU (Senior Member, IEEE) was born in Pucheng, China, 1990. He received the B.S., M.S., and Ph.D. degrees in electrical engineering from Northwestern Polytechnical University (NWPU), Xi'an, China, in 2012, 2015, and 2018, respectively.

From 2017 to 2018, he was with the Department of Electrical Engineering, Electronics and Computer Science, University of Liverpool (UoL), U.K., as an Honorary Academic Researcher. Currently, he is an Associate Research Fellow with the Department of Electrical Engineering, NWPU. His research interests include hybrid-fault-tolerant control techniques for permanent magnet synchronous motor drives, aging issue for motor drives, and power electronics converters and control.

YIHUA HU (Senior Member, IEEE) received the B.S. degree in electrical engineering and the Ph.D. degree in power electronics and drives from the China University of Mining and Technology, in 2003 and 2011, respectively. From 2011 to 2013, he was with the College of Electrical Engineering, Zhejiang University, as a Postdoctoral Fellow. From 2013 to 2015, he was a Research Associate with the Power Electronics and Motor Drive Group, University of Strathclyde. From 2016 to 2019, he was a Lecturer with the Department of Electrical Engineering and Electronics, University of Liverpool (UoL). Currently, he is a Reader with the Electronics Engineering Department, University of York (UoY). He has published over 120 articles in IEEE TRANSACTIONS journals. His research interests include renewable generation, power electronics converters and control, electric vehicle, more electric ship/aircraft, smart energy systems, and non-destructive test technology. He is a fellow of the Institution of Engineering and Technology (FIET). He received the Royal Society Industry Fellowship. He is an Associate Editor of IEEE TRANSACTIONS ON INDUSTRIAL ELECTRONICS, *IET Renewable Power Generation*, *IET Intelligent Transport Systems*, and *Power Electronics and Drives*.